RSC Advances

ROYAL SOCIETY OF CHEMISTRY

www.rsc.org/advances

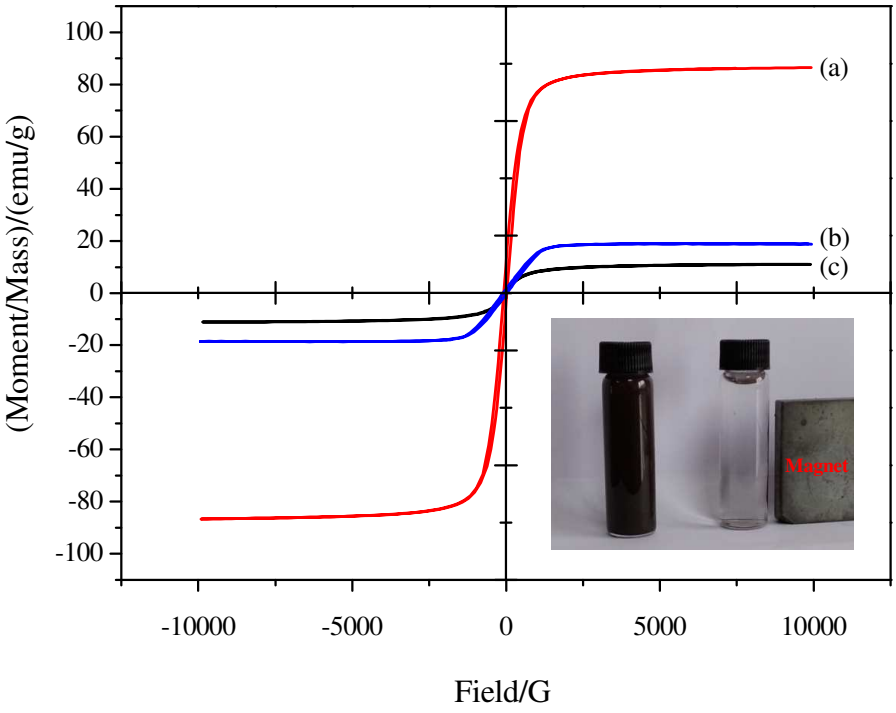

Surface core-shell magnetic polymer modified graphene oxide-based material for 2,4,6-trichlorophenol removal

Mei-Lan Chen[a], Jian-Qing Min[a], Sheng-Dong Pan[b,c], Mi-Cong Jin[b,c]*

([a]College of Biology and Environmental Engineering, Zhejiang Shuren University, Hangzhou 310015, China; [b] Key Laboratory of Health Risk Appraisal for Trace Toxic Chemicals of Zhejiang Province, Ningbo Municipal Center for Disease Control and Prevention, Ningbo, 315010, China; [c]Ningbo Key Laboratory of Poison Research and Control, Ningbo Municipal Center for Disease Control and Prevention, Ningbo, 315010, China)

Abstract: A novel well-designed graphene oxide-based magnetic polymer (GO-Fe_3O_4@P) has been successfully synthesized via distillation-precipitation polymerization, ring-opening and amidation reactions. The as-prepared GO-Fe_3O_4@P was further characterized by transmission electronmicroscopy (TEM), vibrating sample magnetometer (VSM), BET analysis, zeta potential analysis, X-ray photoelectron spectroscopy (XPS), and Fourier transform infrared spectroscopy (FTIR) and the characterization results revealed that core-shell structural Fe_3O_4@P microspheres were covalently bonded onto the GO sheet. The adsorption characteristics of the GO-Fe_3O_4@P intended for removal of 2,4,6-trichlorophenol (2,4,6-TCP) were investigated. Batch adsorption studies were carried out to optimize adsorption conditions. The effect of solution pH, adsorption isotherm, kinetics, and thermodynamics was deeply investigated. The results indicated that the adsorption property of GO-Fe_3O_4@P was highly pH dependent and the adsorption mechanism referred to hydrogen bond and π-π stacking interaction. The adsorption data for 2,4,6-TCP onto GO-Fe_3O_4@P was well fitted to Langmuir isotherm. The maximum adsorption capacity (q_m) of GO-Fe_3O_4@P to

* *Corresponding author, E-mail address: jmcjc@163.com*

2,4,6-TCP was found to be 232.6 mg/g. Kinetic results showed that the adsorption reached equilibrium within 4 min, 10 min, and 60 min for initial 2,4,6-TCP concentrations at 10 mg/L, 100 mg/L, and 500 mg/L, respectively. The data of adsorption kinetics obeyed pseudo-second-order rate model well. Thermodynamic parameters such as ΔH^{θ}, ΔS^{θ}, and ΔG^{θ} for the 2,4,6-TCP adsorption onto GO-Fe_3O_4@P have been estimated, suggesting the adsorption process was endothermic and entropy favored in nature.

Keywords: Graphene oxide-based magnetic polymer (GO-Fe_3O_4@P); Cholorophenols; 2,4,6-TCP; Adsorption

1. Introduction

Cholorophenols are mainly produced in chemical industries such as pretroleum refineries, plastics, pesticides, and pharmaceuticals [1]. The wide use of cholorophenols leads to the inevitable emission and immission into the aquatic environment. 2,4,6-trichlorophenol (2,4,6-TCP) is one of the cholorophenols which is recognized as a toxic, mutagenic and carcinogenic pollutant. It has been reported to cause adverse effects on human nervous system and respiratory problems such as chronic bronchitis, cough and altered pulmonary function [2]. Because of its high toxicity, carcinogenic properties, structural stabilization and persistence in the environment, the removal of 2,4,6-TCP from the environment is crucial.

Recently, many treatment methods have been developed to remove 2,4,6-TCP from aqueous solutions, including photochemical treatment [3], biological treatment [4], and adsorption technology [5-8]. Among these methods, the adsorption approach has been considered as a promising method since it can effectively remove pollutants by

convenient design and operation. Various adsorbents such as montmorillonite [5], activated carbon [6, 7], carbon nanotubes [8] have been applied to remove 2,4,6-TCP from environmental water. However, some of them show low adsorption capacity. Graphene (G) has attracted great attention to researchers due to its extraordinary properties [9]. Especially the large delocalized π-electron system and ultrahigh specific surface area of G make it a promising candidate with strong affinity and high adsorption capacity for carbon-based ring structures [10-12]. However, it is difficult to produce and process on large scales for G. Chemically modified forms of G, such as graphene oxide (GO), may provide an alternative [13]. GO can be well-dispersed in water for its abundant hydrophilic groups, such as hydroxyl, epoxide and carboxylic groups, on its surface [14].

Another fatal problem for GO as an adsorbent is that it is difficult to separate GO from solution via centrifugation after adsorption due to its light weight. The introduction of magnetic composite into GO would effectively solved the above problem since magnetic GO composites could combine the high adsorption capacity of GO and the separation convenience of magnetic materials under magnetic field [15-18]. Herein, in this work, we successfully synthesized a novel graphene oxide-based magnetic polymer (GO-Fe_3O_4@P). The TEM, VSM, and FTIR characterization results showed that the core-shell structural Fe_3O_4@P microspheres were covalently bonded onto the GO sheet. Furthermore, the as-prepared GO-Fe_3O_4@P showed high adsorption capacity toward 2,4,6-TCP and the adsorption mechanism was deeply investigated.

2. Experimental

2.1. Materials

Analytical grade of iron (III) chloride hexahydrate ($FeCl_3 \cdot 6H_2O$), sodium acetate anhydrous (NaAc), ethylene glycol (EG) and sodium hydroxide (NaOH) were purchased from Sinopharm Chemical Reagent Co., Ltd. (Shanghai, China). Divinylbenzene (DVB, purity>99%), glycidylmethacrylate (GMA, purity>99%), and diethylenetriamine (DETA, purity>99%) were supplied by Alddin Chemical Reagent Co., Ltd. (Shanghai, China) and purified by vacuum distillation. 2,2-azobisisobutyronitrile (AIBN, purity>99%) was purchased from J&K Chemical and used as an initiator without further purification. Analytical grade of N-ethyl-N′-(3-(dimethylamino) propyl) carbodiimide (EDC) and N-hydroxysuccinimide (NHS) were obtained from Tokyo Chemical Industry Co., Ltd (Tokyo, Japan). 2,4,6-TCP (purity>99%) was supplied by Aladdin Chemical Reagent Co., Ltd. (Shanghai, China). Chromatographic grade of methanol, acetonitrile and formic acid were obtained from Merck (Darmstadt, Germany).

2.2 GO-Fe_3O_4@P preparation

The synthesis procedure of GO-Fe_3O_4@P was as following: firstly, the magnetic Fe_3O_4 was prepared by solvothermal method according to the literature with a minor modification [19]. Briefly, $FeCl_3 \cdot 6H_2O$ (2.0 g) was dissolved in EG (40 g) to form a clear solution, followed by the addition of NaAc (3.3 g) and polyethylene glycol (1.0 g). The mixture was stirred vigorously for 0.5 h at room temperature and then transferred to a teflon-lined stainless-steel autoclave (50 mL capacity). The autoclave was heated to and maintained at 200 ^{o}C for 10 h and then naturally cooled to room temperature. The black magnetic Fe_3O_4 particles were obtained and washed three times with methanol under ultrasonic conditions to remove the adsorbed solvent.

Then, the core-shell magnetic Fe_3O_4 polymers (Fe_3O_4@P) were synthesized by

distillation-precipitation polymerization as following: 0.05 g of Fe_3O_4 particles was dispersed in 80 mL of acetonitrile solution containing DVB (0.5 g), GMA (0.5 g), and AIBN (0.02 g, 2% wt% of the total monomers). After being degassed with nitrogen for 0.5 h, the reaction mixture was heated from ambient temperature to boiling within 40 min. The polymerization was continued under distillation and was ended after 40 mL of acetonitrile was distilled from the reaction system within 2 h. The final products were collected by magnetic separation and washed three times with deionized water and ethanol, and then dried in a vacuum oven at room temperature for 12 h. Subsequently, the NH_2-functionalized magnetic Fe_3O_4 polymers (Fe_3O_4@P-NH_2) could be easily obtained via ring-opening reaction with DETA in methanol medium for 3 h.

Finally, the GO-Fe_3O_4@P was synthesized via amidation reaction under ambient conditions. Briefly, 20 mg of GO in 20 mL water was ultrasonicated for 2 h, and then 100 mg of EDC and 80 mg of NHS were added into the GO solution. The above mixture was further stirred for 0.5 h to activate carboxyl groups of GO. Next, 0.5 g of Fe_3O_4@P-NH_2 was added into the suspension and ultrasonicated for another 0.5 h. the GO-Fe_3O_4@P was obtained after the reaction carried out at 60 ^oC for 1 h under strong stirring. The product was separated from reaction mixtures by using external magnetic force, and finally dried under vacuum at room temperature for further use.

2.3 Characterizations

The morphology, structure and composition of the GO-Fe_3O_4@P were investigated by TEM (Hitachi, Japan), vibrating sample magnetometer (VSM, Lake Shore 7410), and Fourier Transform Infrared spectrometer (FTIR, Thermo Nicolet, USA). Zeta potential was measured by a Malvern zetameter (Zetasizer 2000). BET analysis was performed on

micromeritics ASAP 2020 surface area and porosityanalyzer (Quantachrome, United States). The X-ray photoelectron spectroscopy (XPS, AXIS ULTRADLD) were used to investigate the adsorption mechanism of 2,4,6-TCP onto GO-Fe_3O_4@P. The fluorescence properties of GO-Fe_3O_4@P, and GO-Fe_3O_4@P-TCP (after 2,4,6-TCP loading) were measured on a fluorescence spectroscopy (Hitach F4500). 100.0 mg of each solid sample were immobilized on a sample holder and measured by emission scan at 320 nm of fixed excitation wavelength.

2.4 Adsorption experiments

Batch adsorption experiments were carried out in 150 mL stoppered flasks, and each of them contained 40 mL of 2,4,6-TCP solution. The solution pH was adjusted by 0.1 mol/L HCl or 0.1 mol/L NaOH, and then 20 mg of adsorbents were added into each flask and shaken at 180 rpm in a thermostatic shaker. The 2,4,6-TCP concentration in the supernatant was measured by HPLC (Agilent 1100 series). According to the 2,4,6-TCP concentrations before and after adsorption, the equilibrium adsorption capacity (q, mg/g) of 2,4,6-TCP bound to the MGO@MIP is calculated using Eq. (1):

$$q_e = \frac{(C_0 - C_e)V}{m} \quad (1)$$

where C_0 and C_e represent the initial solution concentration and the equilibrium concentration of 2,4,6-TCP (mg/L), V is the volume of the 2,4,6-TCP solution (mL), m is the adsorbent dosage (mg), the same hereinafter.

To investigate the effect of pH, 40 mL of 100 mg/L and 500 mg/L 2,4,6-TCP with pH ranging from 2.0 to 10.0 were mixed with 20 mg of magnetic adsorbents for 1 h at 308 K, respectively.

The adsorption isotherm studies were investigated with GO-Fe_3O_4@P initial

concentration ranging from 10 to 500 mg/L, under pH 5.0 at 308 K for 1 h. Langmuir model (Eq. (2)) was applied to analyze the adsorption data.

$$\frac{C_e}{q_e} = \frac{1}{K_L q_m} + \frac{C_e}{q_m} \quad (2)$$

where q_m and K_L are the Langmuir constants related to the maximum adsorption capacity and apparent heat change, respectively.

In the kinetic experiments, the GO-Fe_3O_4@P was also investigated with contacting time ranging from 1 to 180 min at pH 5.0. The pseudo-first-order model (Eq. (3)) [20] and pseudo-second-order model (Eq. (4)) [21] were used to fit the experimental data.

$$\log(q_e - q_t) = \log q_e - (\frac{k_1}{2.303})t \quad (3)$$

$$\frac{t}{q_t} = \frac{1}{k_2 q_e^2} + (\frac{1}{q_e})t \quad (4)$$

where q_t is the adsorption capacity at time t (mg/g), k_1 (min^{-1}), k_2 (g/(mg·min) are the adsorption rate constants.

The thermodynamic studies were carried out at 298, 308, 318, 328, 338, and 348 K, at pH value of 5.0 with 20 mg GO-Fe_3O_4@P used for the treatment of 40 mL of 100 mg/L 2,4,6-TCP solutions.

3. Results and discussion

3.1 Characterization of GO-Fe_3O_4@P

Fig. 1 showed the TEM images of Fe_3O_4@P (Fig. 1a) and GO-Fe_3O_4@P (Fig. 1b). It clearly revealed that well-designed core-shell magnetic Fe_3O_4 polymers (Fe_3O_4@P) could be obtained by distillation-precipitation polymerization, in which the monomers were polymerized and precipitated fast during the distillation of acetonitrile solvent from the

reaction system. It could be obviously seen from Fig. 1a that the uniform polymeric shell of lower image contrast surrounding the inorganic Fe_3O_4 core with narrow size distribution (~600 nm). The TEM image of GO-Fe_3O_4@P exhibited in Fig. 1b showed that Fe_3O_4@P microspheres were covalently bonded on the surface of GO sheet.

FTIR spectroscopy was used to further confirm the synthesis route of GO-Fe_3O_4@P. As shown in Fig. 2a, the characteristic peak of Fe_3O_4 occurs at ~589 cm^{-1}. Other typical peaks could be assigned as follows, v(-OH, -NH_2): ~3400 cm^{-1}; v(-CH_2, -CH_3): ~2921 cm^{-1}, 2853 cm^{-1}; v(-C=O): ~1725 cm^{-1}; δ (-CONH-): ~1636 cm^{-1}; δ(N-H): ~1568 cm^{-1}. These results revealed that magnetic Fe_3O_4@P microspheres were covalently linked to GO sheet via amidation reaction.

The magnetic properties of Fe_3O_4, Fe_3O_4@P and GO-Fe_3O_4@P were tested by VSM shown in Fig. 3. The results indicated that the saturation moments dramatically decreased from 84.4 (Fe_3O_4, Fig. 3a) to 18.7 (Fe_3O_4@P, Fig. 3b) and 11.2 emu/g (GO-Fe_3O_4@P, Fig. 3c) during the preparation processes, implying the successful design and synthesis of GO-Fe_3O_4@P.

Zeta potential of GO-Fe_3O_4@P was measured by dispersing in aqueous solution with pH ranging from 2.0 to 10.0. As shown in Fig. 4 a, the pH_{PZC} (pH of zero point charge) of GO-Fe_3O_4@P was about 4.6. This revealed that the surface of GO-Fe_3O_4@P was positively charged at pH<4.6, confirming the dominant formation of amide groups was $–NH_4^+$ at low pH values. By comparison, the main formation was $–NH_2$ when pH≥5.0. According to the N_2 sorption analysis (Fig. 4b), the BET surface area of GO-Fe_3O_4@P adsorbent is 60.41 m^2/g, and BJH desorption cumulative volume of pores is 0.3428 cm^3/g.

<Insert Fig. 1, Fig.2, Fig. 3 and Fig. 4>

3.2 pH effect and the adsorption mechanism

The effect of pH on the adsorption of 2,4,6-TCP was carried out by varying the solution pH from 2.0 to 10 at initial concentrations of 100 and 500 mg/L, respectively (Fig. 5a). It was noticed that the adsorption capacities of 2,4,6-TCP was highly pH dependent at initial concentrations of 100 mg/L and 500 mg/L. The adsorption increased with the increase of the initial pH, and reached the maximum adsorption capacity at pH 5.0, then sharply decreased with the pH in range of 5.0 to 10.

This could be explained from the perspectives of surface charge of the adsorbent (the data were shown in Fig. 4 a) and the state of 2,4,6-TCP at various pH values. In the present work, the state of 2,4,6-TCP (pKa=6.0) and amide groups on GO-Fe_3O_4@P could be obviously affected by solution pH. At low pH values (pH<5.0), the amide groups on GO-Fe_3O_4@P are easy to protonate and the dominant formation is $–NH_4^+$, which does not have lone pair electrons and was difficult to form hydrogen bond (-O-H···N) with 2,4,6-TCP. Thus, the adsorption capacity was worse than that of pH=5.0, at which the main formation of the surface groups might be $–NH_2$ and it was beneficial to form hydrogen bond (-O-H···N). Meanwhile, when pH>5.0, most of the 2,4,6-TCP molecules presented in an ionic state (deprotonation of hydroxyl group), which resulted in difficulties to form hydrogen bonds (-O-H···N) with amine groups on the surface of GO-Fe_3O_4@P. Furthermore, high adsorption capacity could still be obtained (q>50 mg/g) at any pH value due to π-π stacking interaction between the benzene ring of 2,4,6-TCP and GO sheet.

The adsorption mechanism could be confirmed by FTIR, XPS, and fluorescence

spectroscopy. From FTIR spectroscopy shown in Fig. 2b, a new peak located at ~723.1 cm^{-1}, owing to the stretching vibration of C-Cl bond [22], could be observed, suggesting the successful loading of 2,4,6-TCP onto GO-Fe_3O_4@P. Besides, the characteristic peak of N-H bond at ~1568 cm^{-1} shifted to ~1533 cm^{-1}, indicating the formation of hydrogen bond between 2,4,6-TCP and $–NH_2$ groups on GO-Fe_3O_4@P [23]. It was worth noting that the peaks at 1460 cm^{-1} and 1391 cm^{-1}, due to the skeletal vibration of aromatic C=C bonds, shifted to ~1431 cm^{-1} and 1362 cm^{-1}, respectively, confirming the π-π stacking interactions were formed between the benzene ring of 2,4,6-TCP and the hexagonal skeleton of the GO sheet of GO-Fe_3O_4@P [24]. Furthermore, the hydrogen bond has also been verified by XPS analysis as shown in Fig. 5b. The N1s high-resolution scan of GO-Fe_3O_4@P could be deconvoluted into two individual peaks at binding energies of 398.9 eV and 396.6 eV, which could be assigned to C-N, and N-H, respectively. After 2,4,6-TCP adsorption, the binding energy of N-H bond shifted to 398.5 eV, which may be due to the formation of hydrogen bond between 2,4,6-TCP and the amine groups on the surface of GO-Fe_3O_4@P. The π-π stacking interaction could also be confirmed by fluorescence spectroscopy as shown in Fig. 5c. The results indicated that the fluorescence intensities at 392 nm of GO-Fe_3O_4@P were quenched a lot after 2,4,6-TCP adsorption, implying the π-π stacking interaction appeared between 2,4,6-TCP and GO-Fe_3O_4@P. It was worthwhile to note that the degree of fluorescence-quenching increased with the increase of 2,4,6-TCP loading onto GO-Fe_3O_4@P.

<Insert Fig. 5>

3.3 Effect of initial concentration and adsorption isotherms

The effect of the concentration of 2,4,6-TCP on GO-Fe_3O_4@P was carried out by varying initial concentrations from 10 mg/L to 500 mg/L at 308 K, pH 5.0. The results were shown in Fig. 6 a. It was obviously noticed that the adsorption capacity of 2,4,6-TCP firstly increased with the increasing of the initial 2,4,6-TCP concentrations, and then reached a platform when C_0>250 mg/L.

<Insert Fig. 6>

As it was clearly shown in Fig. 6b, the experimental data of 2,4,6-TCP adsorption were correlated well with the Langmuir isotherm equation as: $C_e/q = 0.0043\ C_e + 0.1060$ ($R^2 = 0.9993$). The q_m and K_L values calculated from the equation were found to be 232.6 mg/g and 0.0406 L/mg, respectively. The fundamental characteristics of Langmuir equation could be interpreted in terms of a dimensionless constant separation factor R_L, defined as $R_L=1/(1+K_LC_0)$, where K_L is Langmuir constant, and C_0 is initial concentration of 2,4,6-TCP. The value of K_L indicated the types of Langmuir isotherm of irreversible (R_L=0), favorable (0<R_L<1), linear (R_L=1), or unfavorable (R_L>1). By calculation, R_L was between 0 and 1 for the present GO-Fe_3O_4@P with any initial concentration of 2,4,6-TCP. For instance, for the initial concentration of 2,4,6-TCP at 100 mg/L, the R_L was 0.1976, which indicated that the adsorption isotherm obeyed the Langmuir model.

3.4 Kinetic studies

The kinetic studies of 2,4,6-TCP were carried out at initial concentrations of 10, 100 and 500 mg/L, pH of 5.0 and at 308 K. The experimental results were presented in Fig. 7. As shown in Fig. 7, compared to the initial concentration at 100 mg/L and 500 mg/L, the

adsorption process is much faster for the initial concentration at 10 mg/L, whose equilibrium time required for the adsorption of 2,4,6-TCP onto GO-Fe_3O_4@P was only 4 min while 10 min and 60 min for 100 mg/L and 500 mg/L. This is because enough active sites located on the surface of GO-Fe_3O_4@P for low concentration of 2,4,6-TCP adsorption. Besides, the kinetic curve of C_0=500 mg/L could be divided into three portions, which could be described by intraparticle diffusion model and indicated that the intraparticle process [25] might be one of the rate-limiting steps for 2,4,6-TCP at 500 mg/L. Unlike C_0=500 mg/L, the kinetic curves of C_0=10 mg/L and 100 mg/L could only be divided into only two portions, thus, the intraparticle process might not be involved in the rate-limiting steps. The probable reason was that, for 2,4,6-TCP adsorption at high concentration, there were not enough active sites on the surface of GO-Fe_3O_4@P and 2,4,6-TCP molecules may migrate to the active groups embedded inside the adsorbent.

Pseudo-first-order and pseudo-second-order models were used to describe the adsorption kinetic data. The correlation coefficient values indicated a better fit of the pseudo-second-order model with the experimental data compared to the pseudo-first-order for all the three concentrations (Table 1). The calculated q_e values were in agreement with the theoretical ones, and the plots showed good linearity with R^2 above 0.9998. Therefore, the adsorption behaviors followed the pseudo-second-order model, suggesting a chemisorption process [26, 27].

<Insert Fig. 7 and Table 1>

3.5 Thermodynamic studies

The thermodynamic parameters, including standard free energy ($\triangle G^{\theta}$), enthalpy

change ($\triangle H^{\theta}$), and entropy change ($\triangle S^{\theta}$), were estimated to evaluate the feasibility and exothermic nature of the adsorption process. The Gibb's free energy change of the process is related to equilibrium constant by Eq. (5):

$$\Delta G^{\theta} = -RT \ln K_D \quad (5)$$

Where K_D is the distribution coefficient, which is defined as Eq. (6):

$$K_D = \frac{q_e}{C_e} = \frac{\text{Amount of 2,4,6-TCP adsorbed on GO-Fe}_3\text{O}_4\text{@P}}{\text{Amount of 2,4,6-TCP in solution}} \times \frac{V}{m} \quad (6)$$

According to thermodynamics, the Gibb's free energy change ($\triangle G^{\theta}$) is also related to the enthalpy change ($\triangle H^{\theta}$) and entropy change ($\triangle S^{\theta}$) at constant temperature by Eq. (7):

$$\Delta G^{\theta} = \Delta H^{\theta} - T\Delta S^{\theta} \quad (7)$$

Thus,

$$\ln K_D = \frac{\Delta S^{\theta}}{R} - \frac{\Delta H^{\theta}}{RT} \quad (8)$$

The values of enthalpy change ($\triangle H^{\theta}$) and entropy change ($\triangle S^{\theta}$) were calculated from the slope and intercept of the plot of ln (q/C_e) *vs* (1/T). The results were shown in Fig. 8. These thermodynamic parameters were listed in Table 2. As shown in Table 2, the enthalpy change ($\triangle H^{\theta}$) for the 2,4,6-TCP adsorption was found to be 13.51 KJ/mol, which indicated that the adsorption was endothermic. The entropy change ($\triangle S^{\theta}$) was 51.85 J/(mol·K). The values of $\triangle G^{\theta}$ were all negative at the studied temperatures, implying the spontaneous nature of the adsorption process.

<Insert Fig. 8 **and Table 2>**

3.6 Adsorbent stability, reuse experiments, and adsorption comparison

The stability of GO-Fe_3O_4@P in the solution was studied by measuring the leaching amount of Fe after the same procedure of adsorption studies of deionized water at pH ranging from 2.0 to 10.0 as described in section 2.4. The residue concentration of Fe ions in the post-treatment water was tested by a spectrophotometer according to the standard colorimetric method [28]. The results showed that it is free from Fe ions in the post-treatment water. The Fe_3O_4 was completely covered with polymer shell, and the present GO-Fe_3O_4@P was stable during the studied pH condition.

The reusability of the GO-Fe_3O_4@P was evaluated by comparing the adsorption capacity. The 2,4,6-TCP loaded GO-Fe_3O_4@P was extracted with methanol-ammonia (95:5, v/v) for 0.5 h after use, and then repeatedly used for 2,4,6-TCP adsorption to determine the adsorption capacity. As shown in Fig. 9, it indicated that GO-Fe_3O_4@P could be used for 8 times with an average loss of less than 4.1%, which implied desired reuse.

The adsorption efficiency of GO-Fe_3O_4@P toward 2,4,6-TCP was compared with other adsorbents in the reported literatures [7, 29-32] as listed in Table 3. The results indicated that the as-prepared GO-Fe_3O_4@P in this work indicated a higher adsorption capacity than those of most adsorbents reported in the literatures as well as a short adsorption equilibration time. Therefore, the newly prepared GO-Fe_3O_4@P has promising potential applications in the removal of 2,4,6-TCP from environmental water.

<Insert Fig. 9 and Table 3>

4. Conclusions

In this work, a novel well-designed graphene oxide-based magnetic polymer

(GO-Fe_3O_4@P) has been successfully prepared via distillation-precipitation polymerization, ring-opening and amidation reactions. The as-prepared MGO@MIP showed desirable levels of magnetic responsibility and chemical stability. Furthermore, the adsorption behaviors of the GO-Fe_3O_4@P intended for removal of 2,4,6-TCP were investigated. The kinetic studies revealed that the adsorption of 2,4,6-TCP onto GO-Fe_3O_4@P followed pseudo-second-order model. Thermodynamic studies suggested that the adsorption processes of 2,4,6-TCP onto the GO-Fe_3O_4@P were endothermic and entropy favored in nature. The adsorption data was well fitted to Langmuir isotherm with maximum adsorption capacity (q_m) at 232.6 mg/g. As a conclusion, the proposed GO-Fe_3O_4@P showed great potential for the removal of 2,4,6-TCP in aqueous solutions.

Acknowledgements

We would like to thank the National Natural Science Foundation of China (No. 21377114), Ningbo Natural Science Foundation of China (No. 2013A610242, No. 2013A610243), Zhejiang Provincial Natural Science Foundation of China (LY14B070004 and LZ14B070001), the Medical Health Foundation for Key Talents in Zhejiang Province, China (No.2013KYA187), the Constructive Major Project for the Department of Health and Family Planning Commission–Zhejiang Province (2014PYA019) and Zhejiang Provincial Program for the Cultivation of High-level Innovative Health Talents for their financial support of this research.

References

[1] H. Zaghouane-Boudiaf, and M. Boutahala, *Chem. Eng. J.,* 2011, 170, 120.

[2] J. Fan, J. Zhang, C. Zhang, L. Ren, and Q. Shi, *Desalination*, 2011, 267, 139.

[3] Z. Xiong, Y. Xu, L. Zhu, and J. Zhao, *Langmuir*, 2005, 21, 10602.

[4] S. Eker, and F. Kargi, *J. Environ. Manage*., 2009, 90, 692.

[5] S. Polati, F. Gosetti, V. Gianotti, and M. C. Gennaro, *J. Environ. Sci. Health Part B*, 2006, 41 765.

[6] B. H. Hameed, I.A.W. Tan, and A. L. Ahmad, *Chem. Eng. J*., 2008, 144, 235.

[7] B. H. Hameed, I.A.W. Tan, and A. L. Ahmad, *J. Hazard. Mater.,* 2009, 164, 1316.

[8] G. C. Chen, X. Q. Shan, Y. S. Wang, B. Wen, Z. G. Pei, Y. N. Xie, T. Liu, and J. J. Pignatello, *Water Res.*, 2009, 43, 2409-2418.

[9] K. S. Novoselov, A. K. Geim, S. V. Morozov, D. Jiang, Y. Zhang, S. V. Dubonos, I. V. Grigorieva, and A. A. Firsov, *Science*, 2004, 306, 666.

[10] M. Hou, X. Zang, C. Wang, and Z. Wang, *J. Sep. Sci.,* 2013, 36, 3242.

[11] Y. Yao, S. Miao, S. Liu, L. P. Ma, H. Sun, and S. Wang, *Chem. Eng. J*., 2012, 184, 326.

[12] L. Ai, C. Zhang, and Z. Chen, *J. Hazard. Mater.*, 2011, 192, 1515.

[13] R. S. Ruoff, *Nat Nanotechnol*, 2008, 3, 10.

[14] O. Akhavan, *Carbon*, 2011, 49, 11.

[15] K. R. Parmar, I. Patel, S. Basha, and Z. V. P. Murthy, *J. Mater. Sci.*, 2014, 49, 6772.

[16] J. Zhu, S. Wei, H. Gu, Sowjanya B. Rapole, Q. Wang, Z. Luo, N. Haldolaarachchige, David P. Young, and Z. Guo, *Environ. Sci. Technol.*, 2011, 46 977.

[17] C. Shi, J. Meng, and C. Deng, *Chem. Commun*., 2012, 48, 2418.

[18] F. He, J. Fan, D. Ma, L. Zhang, C. Leung, and H. L. Chan, *Carbon*, 2010, 48, 3139.

[19] H. Deng, X. Li, Q. Peng, X. Wang, J. Chen, and Y. Li, *Angew Chem. Int. Ed*., 2005, 117,2842.

[20] Y. S. Ho, and G. Mckay, *Water Res.*, 1999, 33, 578.

[21] Y. S. Ho, and G. Mckay, *Process Biochem.*, 1999, 34, 451.

[22] J. Chen, M. A. Hamon, H. Hu, Y. Chen, A. M. Rao, P. C. Eklund, and R. C. Haddon, *Science*, 1998, 282, 95.

[23] L. Zhou, L. Ji, P. C. Ma, Y. Shao, H. Zhang, W. Gao, and Y. Li, *J. Hazard. Mater.*, 2014, 265 104.

[24] Y. Zhang, Y. Tang, S. Li, S. Yu, *Chem. Eng. J.,* 2013,222, 94.

[25] A. Ramesh, H. Hasegawa, W. Sugimoto, T. Maki, and K. Ueda, *Bioresour. Technol.*, 2008, 99, 3801.

[26] G. Crini, H. N. Peindy, F. Gimbert, and C. Robert, *Sep. Purif. Technol.*, 2007, 53, 97.

[27] Y. S. Ho, *J. Hazard. Mater.*, 2006, 136, 681.

[28] B. X. Cai, and Y. W. Chen, Basical Chemistry Experiments, Science Press, Beijing, China, 2001.

[29] B.H. Hameed, *Colloid Surface A*, 2007, 307, 45.

[30] M. Radhika, and K. Palanivelu, *J. Hazard. Mater.*, 2006, 138, 116.

[31] M. M. Mostsa, J. M. Thwala, T. A. M. Msagati, and B. B. Mamba, *Water Air Soil Pollut*, 2012,223, 1555.

[32] A. Denizli, G. Özkan, and M. Uçar, *Sep. Purif. Technol.*, 2001, 24, 255.

Figures and Captions

Fig. 1 TEM images of (a) Fe_3O_4@P, and (b) GO-Fe_3O_4@P

Fig. 2 FTIR curve of GO-Fe_3O_4@P

Fig. 3 VSM images of (a) Fe_3O_4; (b) Fe_3O_4@P; (c) GO-Fe_3O_4@P

Fig. 4 (a) Zeta potential of GO-Fe_3O_4@P; (b) N_2 adsorption–desorption isotherm of GO-Fe_3O_4@P

Fig. 5 (a) Effect of pH on the adsorption of 2,4,6-TCP; (b) high-resolution scan of N1s; (c) fluorescence spectroscopy of: (i) GO-Fe_3O_4@P (ii~v) GO-Fe_3O_4@P adsorbed with different amount of 2,4,6-TCP (initial 2,4,6-TCP concentrations at 10 mg/L, 100 mg/L, 200 mg/L, and 500 mg/L, respectively).

Fig. 6 (a) Adsorption behaviors of 2,4,6-TCP at different initial concentrations; (b) Langmuir adsorption isotherm of 2,4,6-TCP onto GO-Fe_3O_4@P

Fig. 7 Adsorption kinetic of 2,4,6-TCP onto GO-Fe_3O_4@P at different concentrations

Fig. 8 Thermodynamitic study of adsorption of 2,4,6-TCP onto GO-Fe_3O_4@P

Fig. 9 Adsorption capacities of 2,4,6-TCP on GO-Fe_3O_4@P in 8 cycles

Tables and Captions

Table 1 Parameters of pseudo-first-order and pseudo-second-order models for the adsorption of 2,4,6-TCP on GO-Fe_3O_4@P at different initial concentrations

Table 2 Thermodynamic parameters for 2,4,6-TCP adsorption at different temperatures

Table 3 Comparison with the adsorbents for 2,4,6-TCP removal in the literatures

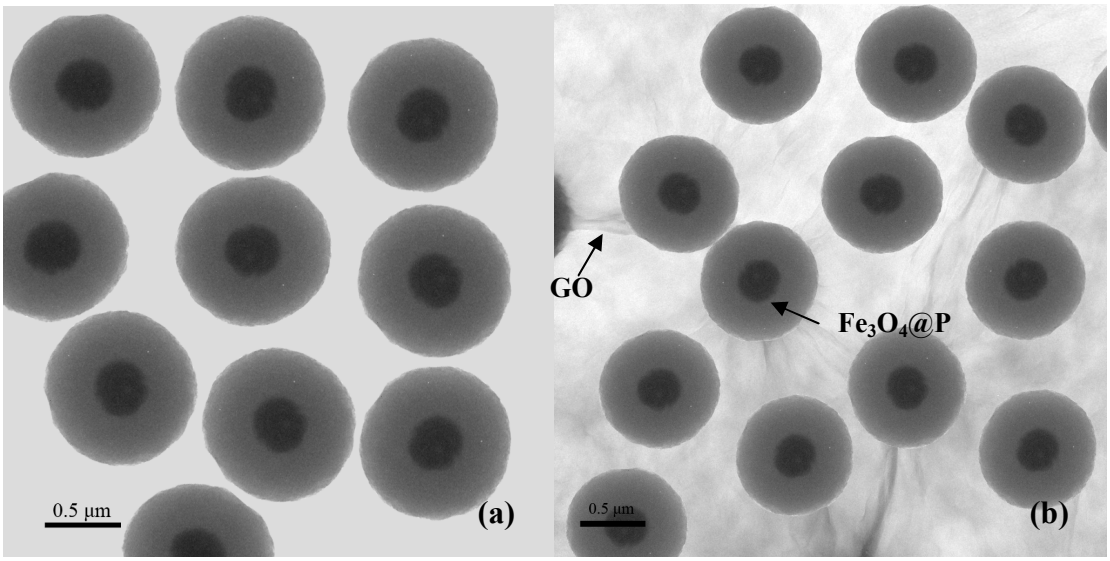

Fig. 1 TEM images of (a) Fe_3O_4@P, and (b) GO-Fe_3O_4@P

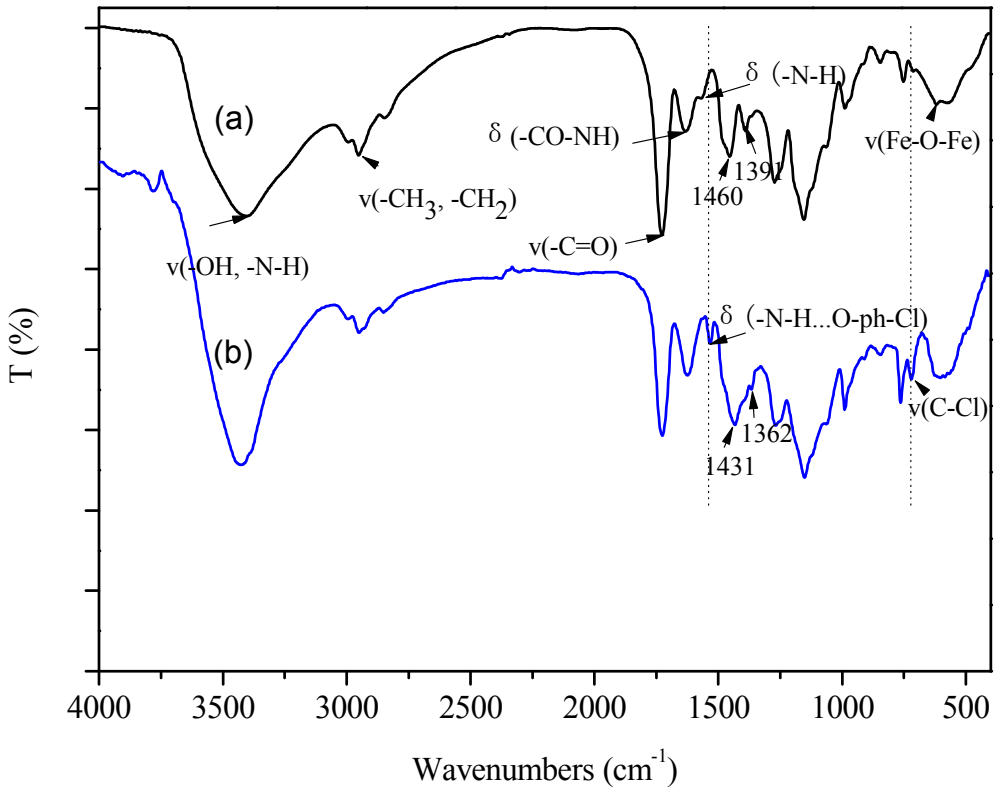

Fig. 2 FTIR curves of (a) GO-Fe_3O_4@P; (b) 2,4,6-TCP adsorbed GO-Fe_3O_4@P

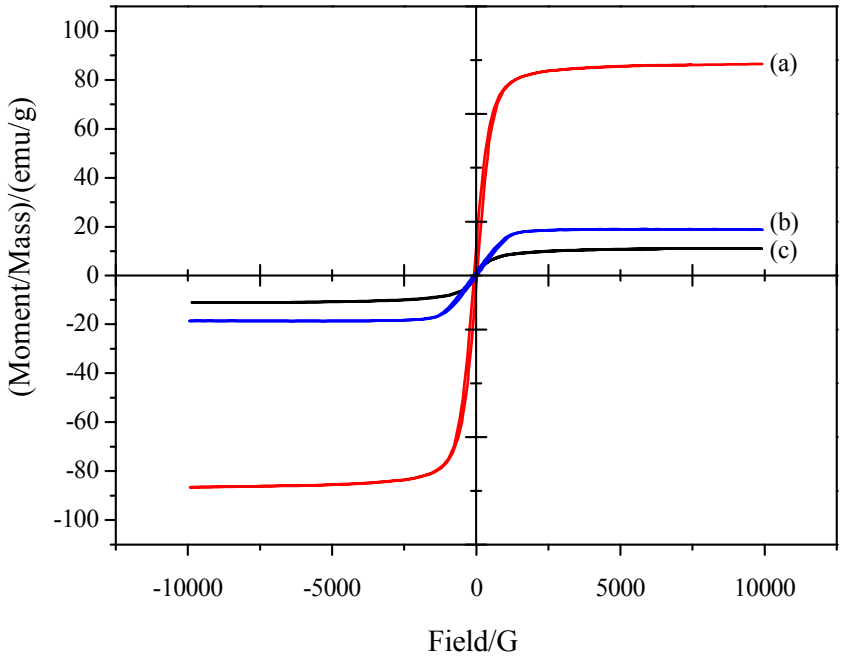

Fig. 3 VSM images of (a) Fe_3O_4; (b) Fe_3O_4@P; (c) GO-Fe_3O_4@P

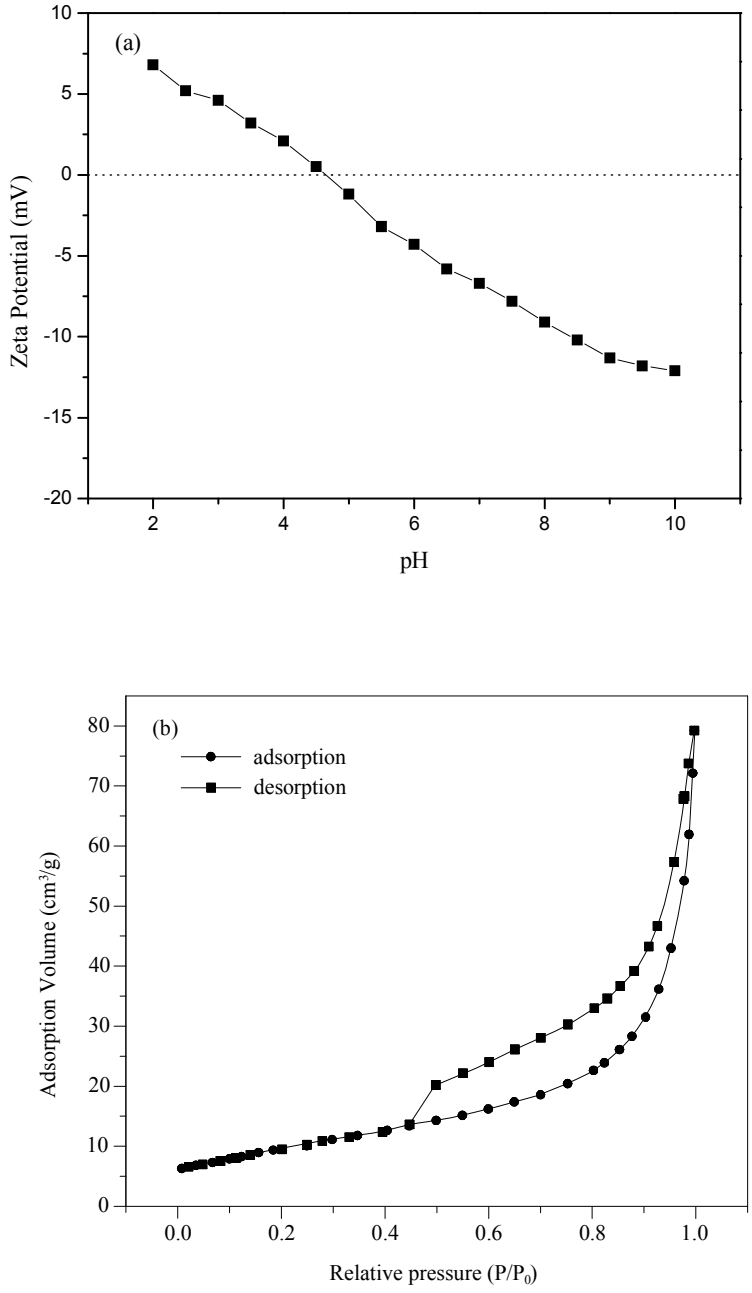

Fig. 4 (a) Zeta potential of GO-Fe_3O_4@P; (b) N_2 adsorption-desorption isotherm of GO-Fe_3O_4@P

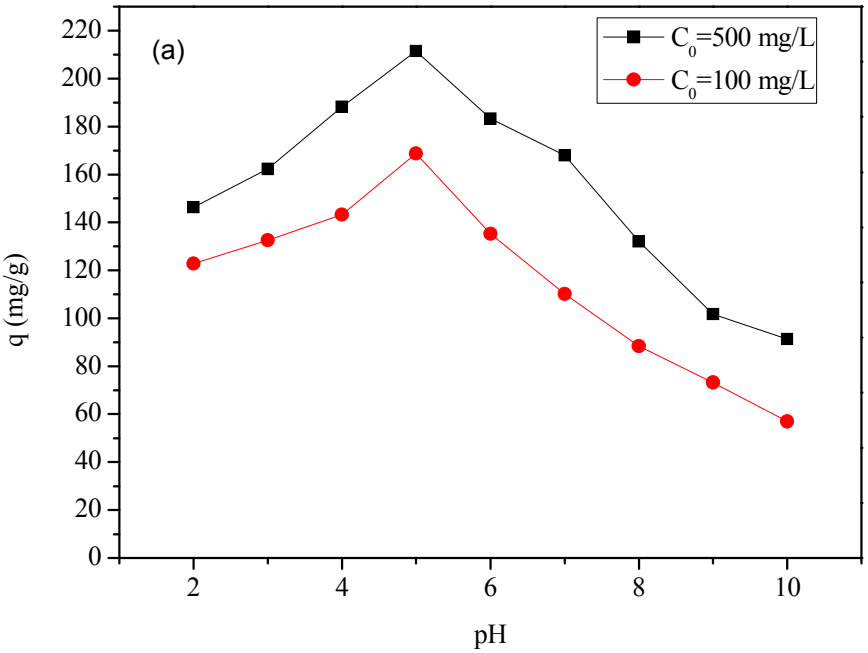

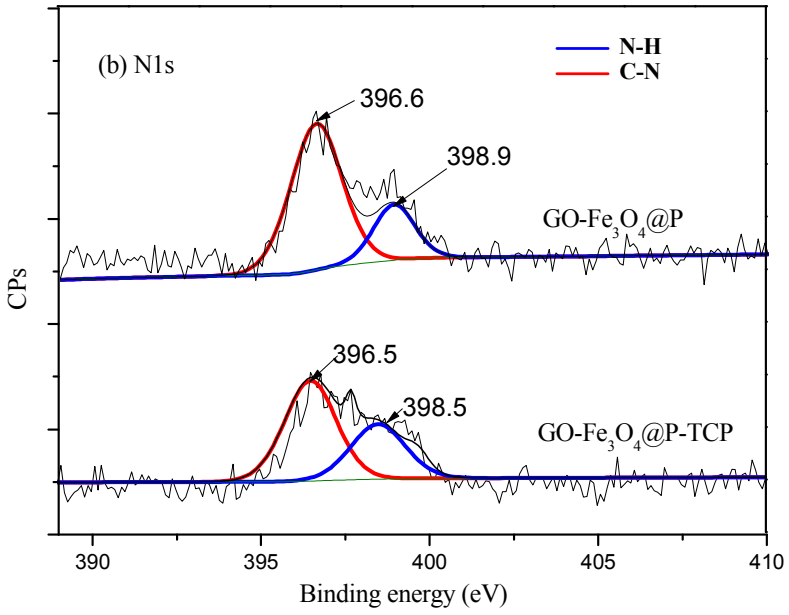

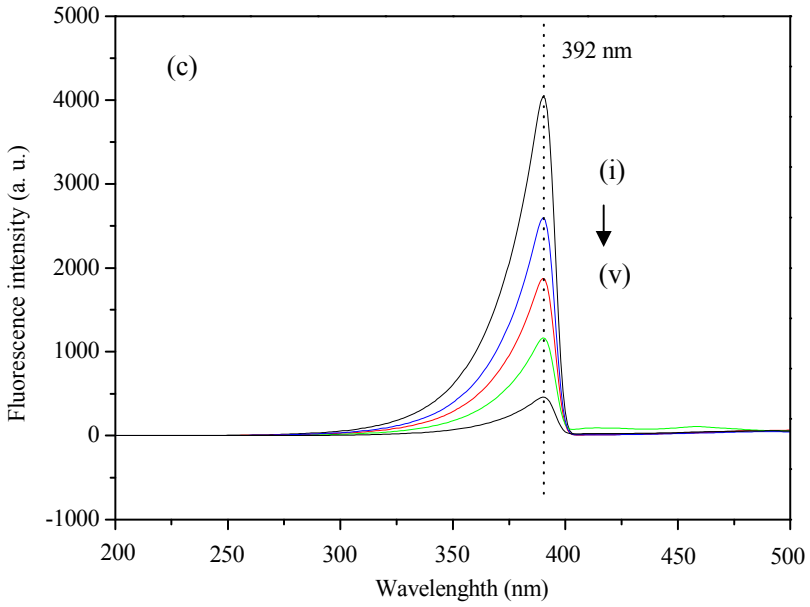

Fig. 5 (a) Effect of pH on the adsorption of 2,4,6-TCP; (b) high-resolution XPS scan of N1s; (c) fluorescence spectroscopy of: (i) GO-Fe_3O_4@P (ii~v) GO-Fe_3O_4@P adsorbed with different amount of 2,4,6-TCP (initial 2,4,6-TCP concentrations at 10 mg/L, 100 mg/L, 200 mg/L, and 500 mg/L, respectively).

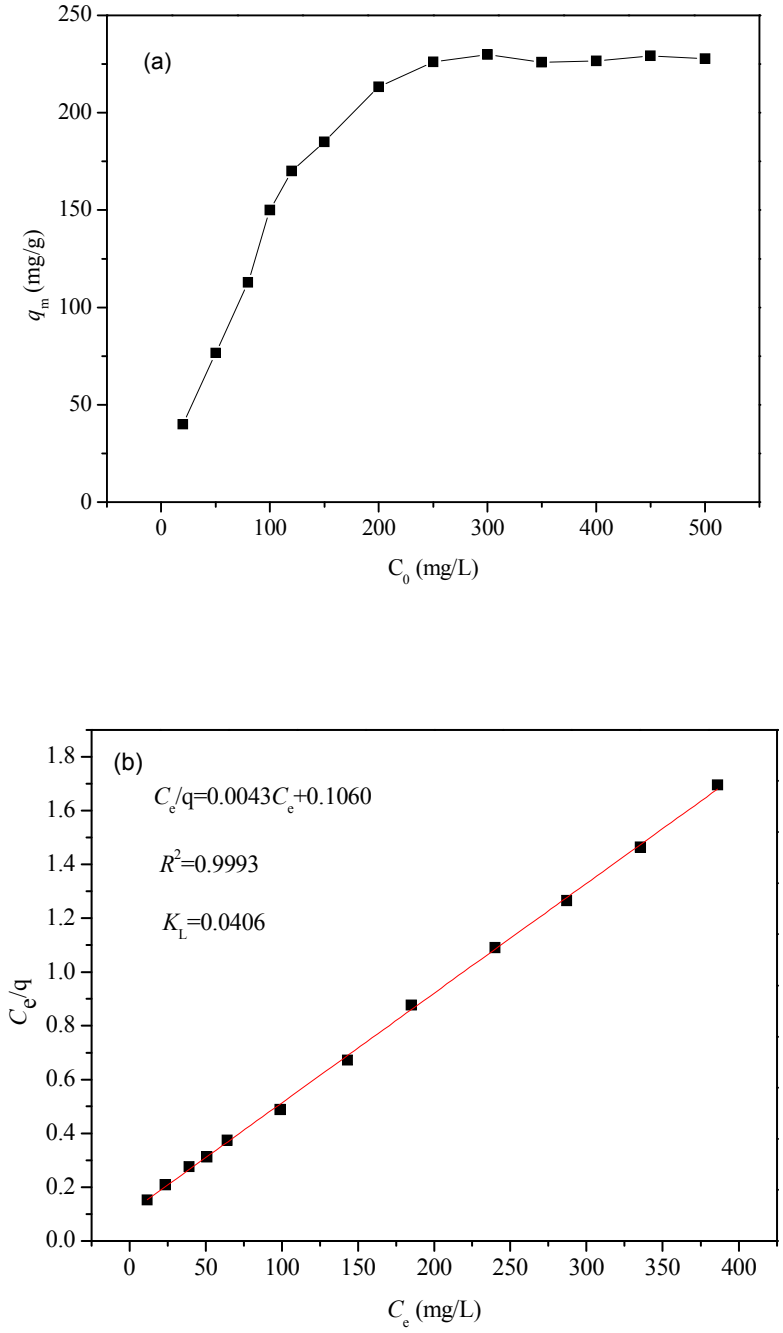

Fig. 6 (a) Adsorption behaviors of 2,4,6-TCP at different initial concentrations; (b) Langmuir adsorption isotherm of 2,4,6-TCP onto GO-Fe_3O_4@P

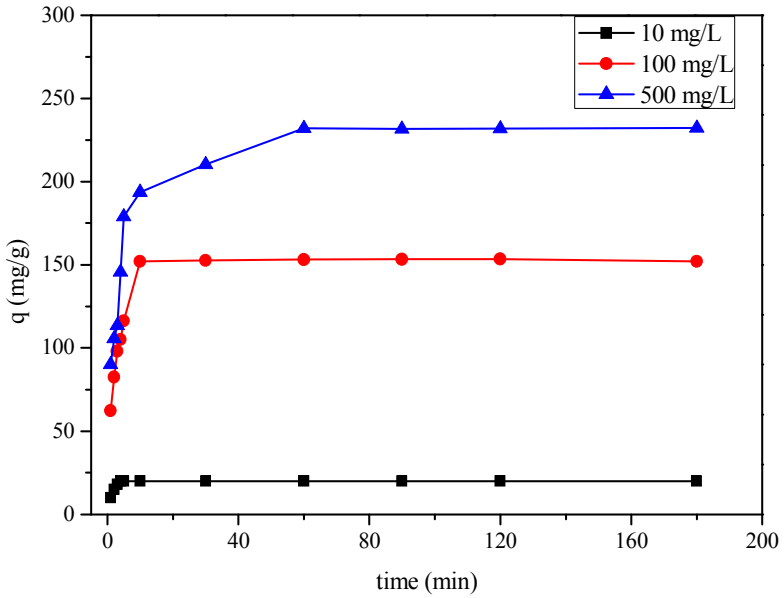

Fig. 7 Adsorption kinetic of 2,4,6-TCP onto GO-Fe_3O_4@P at different concentrations

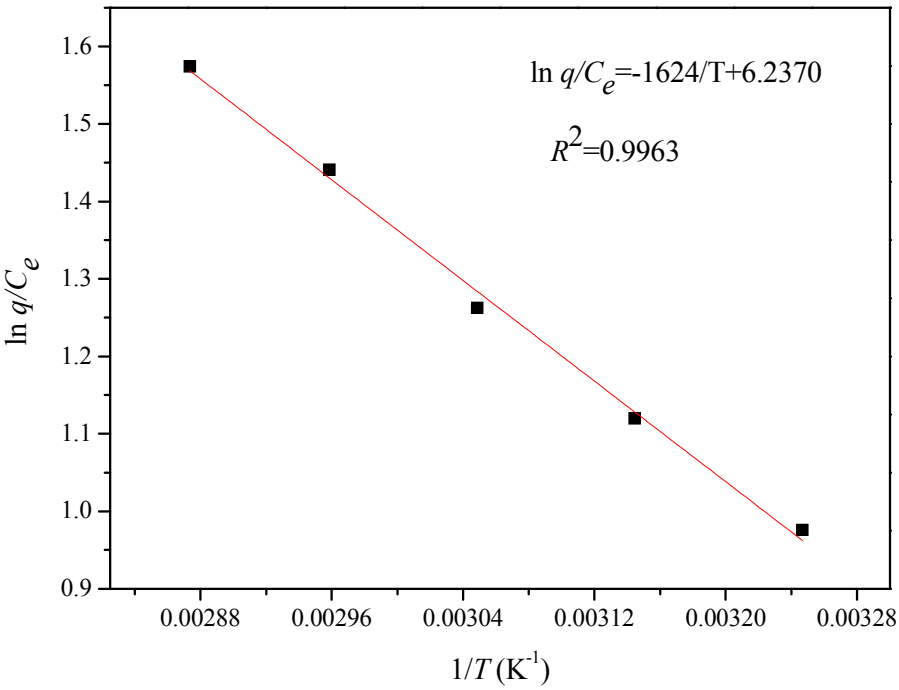

Fig. 8 Thermodynamitic study of adsorption of 2,4,6-TCP onto GO-Fe_3O_4@P

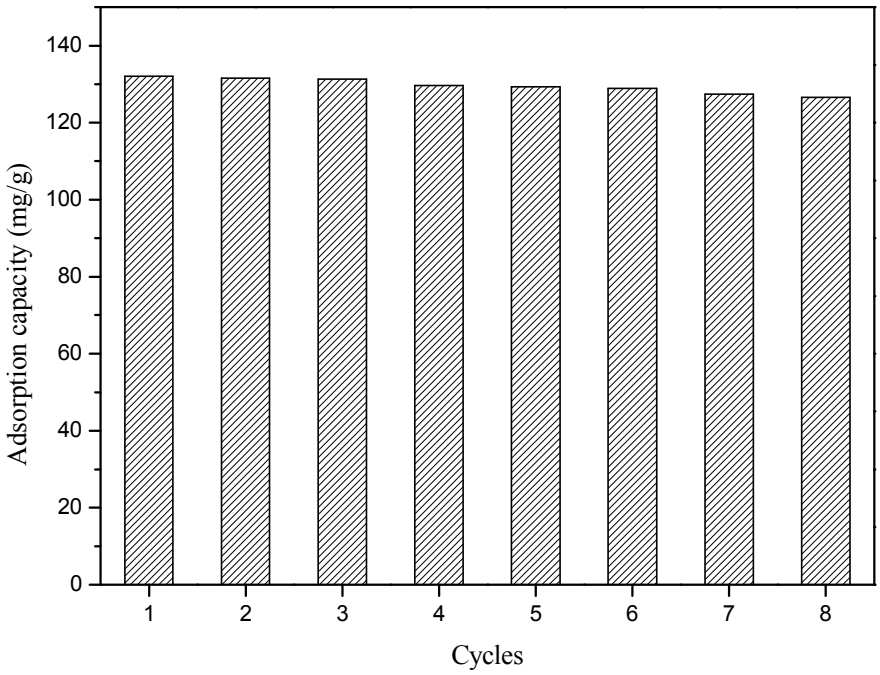

Fig. 9 Adsorption capacities of 2,4,6-TCP on GO-Fe_3O_4@P in 8 cycles

Table 1 Parameters of pseudo-first-order and pseudo-second-order models for the adsorption of 2,4,6-TCP on GO-Fe_3O_4@P at different initial concentrations

Initial concentrations of 2,4,6-TCP (mg/L)	$q_{e,\,exp}$ (mg/g)	Pseudo-first-order model			Pseudo-second-order model		
		k_1(min^{-1})	$q_{e,cal}$(mg/g)	R^2	k_2(g/(mg·min))	$q_{e,cal}$(mg/g)	R^2
10	20.0	0.8049	25.2	0.9572	0.1693	20.0	0.9999
100	151.2	0.4972	196.8	0.9286	0.0058	153.8	0.9998
500	235.2	0.0596	117.4	0.9456	0.0018	238.1	0.9998

Table 2 Thermodynamic parameters for 2,4,6-TCP adsorption at different temperatures

Temperature (K)	q_e (mg/g)	ΔG (kJ/mol)	ΔH (kJ/mol)	ΔS (J/(mol·K))
308	114.0	-2.46		
318	121.0	-2.98		
328	127.7	-3.50	13.51	51.85
338	135.7	-4.02		
348	141.4	-4.53		

Table 3 Comparison with the adsorbents for 2,4,6-TCP removal in the literatures

Adsorbents	Initial concentration (mg/L)	pH value	Equilibrium time (min)	q_m (mg/g)	Ref.
Activated clay	30-220	4.0	30	123.5	[29]
Commercial grade coconut shell-based activated carbon	10-100	2.0	210	112.4	[30]
Surfactant-modified clinoptilolite–polypropylene hollow fibre composites	3-150	4-6	1440 (24 h)	64.1-77.5	[31]
Cibacron Blue F3GA carrying pHEMA microbeads	25-1000 mg/L	6.0	20	186.8 (94.6 μmol/g)	[32]
Palm empty fruit bunch (EFB)-based activated carbon				168.9	[7]
GO-Fe_3O_4@P	10-500	5.0	4-60	232.6	This work